Cloud Clusters and Superclusters over the Oceanic Warm Pool

BRIAN E. MAPES AND ROBERT A. HOUZE, JR.

Department of Atmospheric Sciences, University of Washington, Seattle, Washington

(Manuscript received 17 June 1992, in final form 10 November 1992)

ABSTRACT

Infrared satellite images of the oceanic warm-pool region (80°E–160°W) have been objectively processed to reveal tropical "cloud clusters" with temperatures colder than a given threshold. Cloud clusters span a somewhat lognormal distribution of sizes. The cloudiness per unit size interval peaks at small size, but half of the very cold (<208 K) cloudiness is contributed by cloud clusters greater than 20 000 km^2 in size, while half of the moderately cold (<235 K) cloudiness is contributed by cloud clusters greater than 100 000 km^2 in size.

The diurnal cycle of cold cloudiness is primarily a sun-synchronous process within large and giant clusters, not a modulation of populations of isolated convective clouds. Deep convection in these clusters peaks before dawn and decreases through the morning; then the moderately cold cloud area expands suddenly in the afternoon. Over the maritime continent, an additional diurnal cycle of small clusters is present, with an afternoon pulse of convection over land and a lesser peak in small-cluster convection over the surrounding seas at night.

The eastward-propagating intraseasonal variation (ISV) is apparent in fractional cold cloudiness integrated across the entire tropical latitude belt. The ISV modulates cloud clusters of all sizes, but larger clusters are proportionately more affected than smaller clusters.

Cloud clusters have been tracked in time to reveal "time clusters," which spatially overlap from one frame of imagery to the next. In some cases, convection is so gregarious and interconnected that these time clusters last for more than two days. These cases are called "superclusters." Although they may exist at any given instant as several distinct cloud clusters, these superclusters are apparently real physical entities, as defined by space–time continuity of very cold-topped cloud (proxy for precipitation) area.

1. Introduction

Tropical deep convective clouds are easily identified on infrared (IR) satellite pictures, because of the large temperature difference between the cold upper-tropospheric cloud tops and the much warmer surface and low cloud background. These telltale cold cloud shields or "cloud clusters" span a wide range of sizes, from numerous but small single cumulonimbus clouds to rare but huge clusters with multiple embedded mesoscale precipitation features (Leary and Houze 1979). Cold cloudiness in IR satellite imagery is frequently used to estimate rainfall in climate studies (Janowiak and Arkin 1991). These IR rainfall estimates may in turn be used to fit precipitation relationships with outgoing longwave radiation (OLR), which has the advantage of being measured globally by polar-orbiting satellites. In addition to indicating the location of convective activity, and hence precipitation and latent heating, the upper-tropospheric cloudiness itself has a profound effect on the local radiation budget (Webster and Stephens 1980).

The reliability, availability, and geographical stationarity of IR imagery from geosynchronous satellites make the data easy to analyze. It is particularly simple to construct geographical and diurnal composites (e.g., Janowiak and Arkin 1991; Albright et al. 1985). Another popular analysis technique is to look for zonal motions of cloudiness in time–longitude sections, indicating easterly waves (Chang 1970) or the eastward-propagating intraseasonal variation (ISV) (Nakazawa 1988; Lau et al. 1991).

The aforementioned types of studies use the planetary-scale coverage and high temporal resolution offered by geosynchronous IR satellite imagery. But none fully uses the high spatial resolution (10 km in the present dataset), which reveals much about the mesoscale structure of the cloudiness. There is an extensive paper on a subset of satellite cloud clusters called *mesoscale convective complexes* (MCCs) (Maddox 1980). Laborious manual counts of cold cloud shields exceeding the arbitrary MCC size, shape, and duration cutoffs have been collected (Velasco and Fritsch 1987; Miller and Fritsch 1991). But such studies do not indicate how the large mesoscale systems like MCCs fit into the total cloudiness fields used in rainfall estimates, radiation budgets, and other studies.

Williams and Houze (1987) developed an objective technique to identify and track connected areas of cloudiness with blackbody temperature less than a specified threshold (hereafter called *cloud clusters*). The present study is an application of their technique (with

Corresponding author address: Dr. Robert A. Houze, Jr., Department of Atmospheric Sciences, AK-40, University of Washington, Seattle, WA 98195.

improvements) to a dataset far more extensive in both space and time. The field of view of the Geostationary Meteorological Satellite (GMS) (Fig. 1) extends from the eastern Indian Ocean to about 160°W in the Pacific Ocean. The time periods analyzed include the southern summer season (November–February) of three consecutive years, namely, 1986/87, 1987/88, and 1988/89. The 1986/87 and 1987/88 data periods were characterized by anomalously warm sea surface temperatures in the western equatorial Pacific Ocean, while in 1988/89 the equatorial Pacific was anomalously cool. Two well-defined passages of the ISV were observed in each of the three seasons (section 5). These same three years were also analyzed by Janowiak and Arkin (1991), who have presented mean maps of SST and estimated precipitation.

The objective of this study is to examine the size distributions of cloud clusters, and the temperature distributions within them, as functions of location, year, phase of the ISV, and time of day. In other words, we consider the contributions of cloud clusters of different size classes to the geographical, diurnal, intraseasonal, and interannual variations of total cloudiness.

Section 2 contains a brief review of IR temperature thresholds chosen by various authors for various purposes. Section 3 describes the dataset and outlines the cluster finding and tracking algorithms. Section 4 contains a description of the population of cloud clusters. In section 5, the diurnal cycle of cloudiness as a function of IR temperature and cluster size is discussed. Section 6 deals with the ISV. The results of objectively matching cloud clusters from one satellite picture to the next are presented in section 7, with one of Nakazawa's (1988) "superclusters" analyzed as an example. Conclusions are presented in section 8.

2. IR temperature thresholds

Table 1 lists a number of temperature thresholds from the infrared satellite literature. At the cold end of the range are the −75° and −65°C thresholds used in this study, justified by our subjective impression of an approximate correspondence to radar echo patterns observed in mature nocturnal oceanic mesoscale convective systems (MCSs) during the Equatorial Mesoscale Experiment (EMEX) (Webster and Houze 1991; Mapes and Houze 1992). Williams and Houze (1987) used −60°C on similar grounds. Other thresholds chosen for studies of individual cloud clusters include the −32° and −52°C criteria used by Maddox (1980) to define an MCC. Hand counts of MCCs around the world have been performed by Velasco and Fritsch (1987) and Miller and Fritsch (1991).

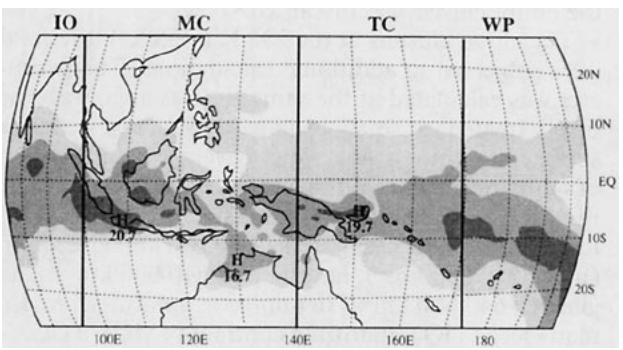

FIG. 1. Base map of the GMS field of view and three-season mean percent high cloudiness (PHC_{228}, the fractional coverage of cloud with infrared temperature less than 228 K). Contour interval is 5%. Vertical lines delineate the four geographical domains: Indian Ocean (IO), maritime continent (MC), TOGA-COARE (TC), and west Pacific (WP).

Fu et al. (1990) chose −58°C as a threshold for tropical "deep convective cloud" on the basis of pixel comparisons with highly reflective cloud in simultaneous visible images. The high cloudiness index used by Nakazawa (1988) and Lau et al. (1991) contains the threshold −48°C. Finally, on the warm end, Arkin (1979) found that a −38°C threshold gave the best linear regression with GATE [GARP (Global Atmospheric Research Program) Atlantic Tropical Experiment] rainfall; this threshold has since been retained in rainfall estimates by Arkin and Meisner (1987) and Janowiak and Arkin (1991). Albright et al. (1985), independent of Arkin, settled on −36°C as the best predictor (in a linear regression sense) of GATE rainfall. Fu et al. (1990) denoted cloud tops from −4° to −58°C "cirrus anvil cloud" (CAC), but they mistakenly related CAC to the stratiform *precipitation* portion of mesoscale convective systems. Stratiform precipitation is included in the radar echo area that we contend is closely related to very cold (−65°C) cloud.

The area covered by cold cloud as a function of temperature threshold is shown in Fig. 2, normalized by the −38°C cloud cover. The solid line, indicating the grand mean, is repeated in all four panels. In general, cloud tops colder than −65°C cover about 20% of the area, with cloud top colder than −38°C. That percentage tended to be smaller over the west Pacific sector in 1988/89 (Fig. 2a), during suppressed phases of the intraseasonal variation (Fig. 2b), in the late afternoon (Fig. 2c), and within smaller cloud clusters (Fig. 2d).

In this study we have chosen primarily to examine cloud clusters as defined by the "very cold" threshold (−65°C), which matches the instantaneous precipitation area in radar-sampled mature MCSs fairly well, and the "moderately cold" (−38°C) threshold used by Arkin and collaborators as an estimator of integrated rainfall amount.

3. Data and methods

The data used in this study are 3-h infrared satellite images from the Japanese GMS satellite, with the full disk of the earth in an 1100-pixel × 1100-pixel array (maximum resolution approximately 9 km at the subsatellite point). A 1040 × 522 subimage covering just

TABLE 1. Infrared temperature thresholds.

T_{BB} (K)	T_{BB} (°C)	Justification or comments	Author(s)
188	(−85)	tropopause temperature in warm-pool sounding	Mapes and Houze 1992
198	(−75)	conservative estimate of EMEX radar echo area	present
208	(−65)	moderate estimate of EMEX radar echo area	present
213	(−60)	winter MONEX radar echo area	Williams and Houze 1987
215	(−58)	"deep convective," highly reflective in visible	Fu et al. 1990
218	(−55)	geographical and diurnal distributions studied	Albright et al. 1985; Keenan et al. 1989; Mapes and Houze 1992
219	(−54)	defines mesoscale convective complex (MCC)	Maddox 1980
225	(−48)	cold cloud index $I_{T_{BB}} = (225 - T_{BB})/5$	Nakazawa 1988; Lau et al. 1991
235	(−38)	optimum linear regression with GATE rainfall	Arkin 1979; Richards and Arkin 1981; Arkin and Meisner 1987
233	(−36)	optimum linear regression with GATE rainfall	Albright et al. 1985
267	(−6)	"cirrus anvil" (mistaken for nimbostratus)	Fu et al. 1990

the tropics (Fig. 1) was copied out of the full image. Navigation information accompanying each image was used to correct for a small diurnal wobble of the location of the earth in the image array. Each pixel in the image contains a number between 0 and 255, which can be converted to equivalent blackbody temperature T_{BB} using a nonlinear conversion table supplied with the data. No drift of the instrument calibration was apparent, so a single conversion table was used on all the data.

The data, catalogued as an International Satellite Cloud Climatology Project (ISCCP) B-1 product, were obtained from the U.S. National Oceanic and Atmospheric Administration Satellite Data Services Division.[1] The dates we have examined are 1 November 1986–28 February 1987, 25 November 1987–29 February 1988, and 16 November 1988–29 January 1989. The years were selected because 1986/87 included the EMEX and the Australian Monsoon Experiment (AMEX) (Webster and Houze 1991; Mapes and Houze 1992), and it was an El Niño year, while 1988/89 was a La Niña (cold western Pacific) year. Also, these three years had been examined by Janowiak and Arkin (1991). The specific periods within each season were selected on the basis of time–longitude sections of OLR, which indicate the phase of the eastward-propagating intraseasonal variation. Each of our three seasons includes two passages of the ISV (section 5). The times of the images varied somewhat, but truncated to the hour they are 0200, 0500, 0800, 1100, 1500, 1700, 2000, and 2300 UTC. Local time at the subsatellite point (140°E) is UTC + 10 h. Many 0200 UTC images are missing ($^{70}/_{281}$ or 25%), while images at the other hours are almost never missing. In the diurnal cycle figures, the appropriate correction factor has been applied to the 0200 UTC cloudiness.

The data processing algorithm, based on the prototype by Williams and Houze (1987), works as follows. Connected areas of cold cloudiness, called *line clusters,* are found within each line (row) of the image array containing one satellite image, or *frame.* The line clusters are then matched from one line to the next. Line clusters on two successive lines must share a column (not merely touch diagonally) to be considered connected. Once the cloud clusters are found, a routine steps through its constituent pixels, summing up the area and calculating the centroid position of each cluster. A more detailed description of a similar cluster-finding algorithm may be found in Wielicki and Welch (1986).

All calculations were performed in the image plane, so no remapping to geographical coordinates was necessary. The sphericity of the earth was accounted for by assigning to each pixel a geographical area of 81 km^2 times a geometrical stretch factor that is a function only of distance from the subsatellite point. This factor varied from 1 (at the subsatellite point) to 3.3 at the edge of the acceptable data area (the edge of Fig. 1). If any part of a cluster extended beyond the 3.3 cutoff, the entire cluster was discarded.

The cloud clusters at the 235 K (−38°C) threshold were subjected to additional calculations. The perimeter was calculated at the same time as area, with the pixels treated as small rectangles (squares, near the subsatellite point). Also, area coverage as a function of temperature within the clusters was tabulated. The resulting temperature histograms were calculated for four cluster size ranges [small (<40 000 km^2), medium (up to 250 000 km^2), large (up to 640 000 km^2), and giant (>640 000 km^2)] in four geographical zones: Indian Ocean (IO), maritime continent (MC), TOGA-COARE[2] domain (TC), and western Pacific (WP), at

[1] Ray Zehr of Colorado State University kindly provided six weeks of data.

[2] Tropical Ocean Global Atmosphere program's Coupled Ocean–Atmosphere Response Experiment.

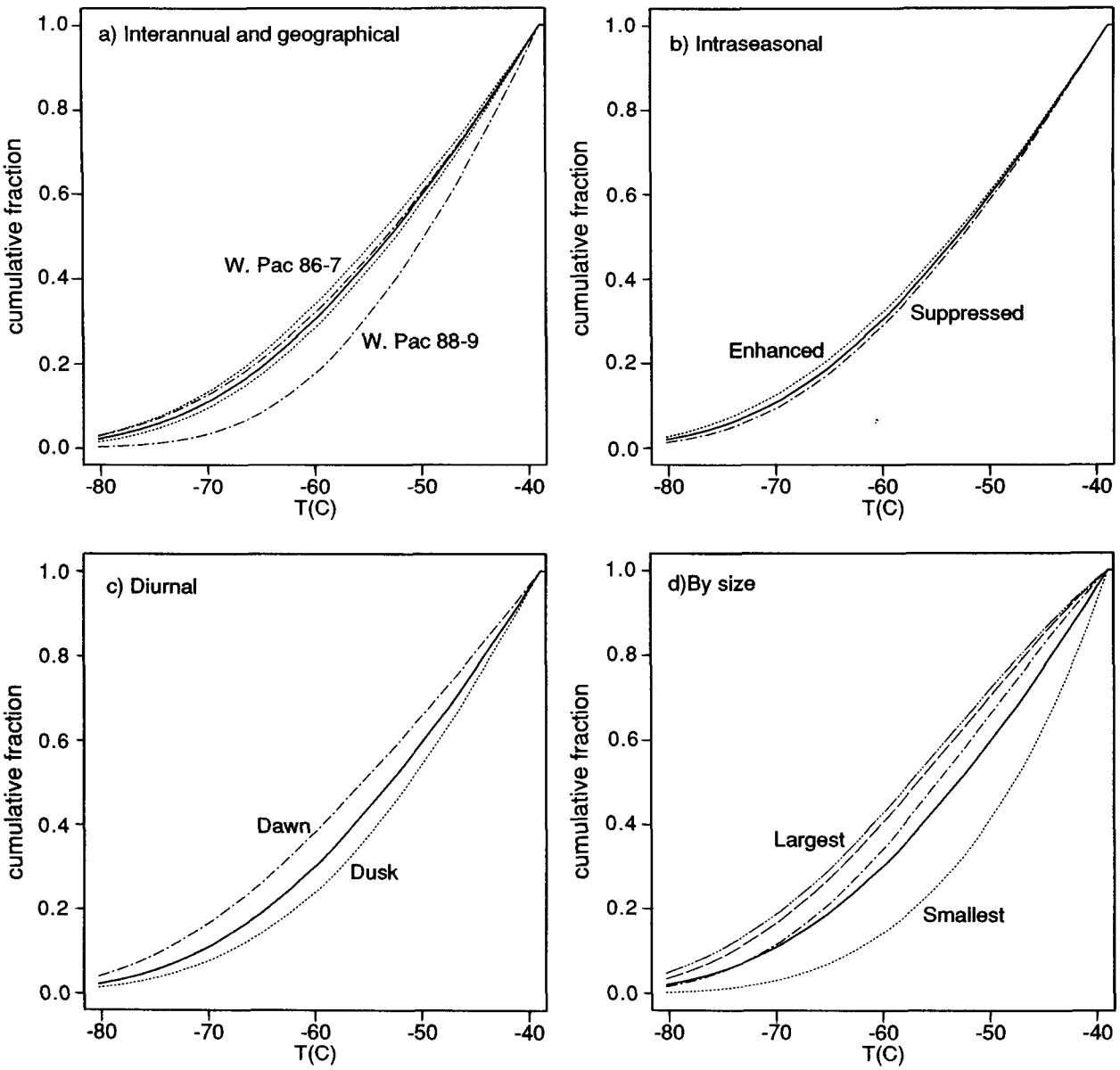

FIG. 2. Fraction of the area of moderately cold (<235 K) cloud that is also colder than the indicated temperature. The solid line is the grand mean, repeated in all panels for comparison. (a) 1986/87 (dot) and 1988/89 (dash-dot) for the WP (labeled) and MC (unlabeled) geographical domains. (b) Intraseasonal enhanced and suppressed composites in the TC domain (see section 6). (c) Dawn and dusk in the TC domain. (d) Size categories: small (<40 000 km^2), medium (up to 250 000 km^2), large (up to 640 000 km^2), and giant (>640 000 km^2).

each of the eight times of day, week by week. This permitted the geographical, diurnal, and intraseasonal variations in cloud-cluster temperature distributions to be subdivided according to cluster size (as shown in Fig. 2).

Williams and Houze (1987) also devised a technique for matching cloud clusters in time, from one frame to the next. In their scheme, the spatial overlap between all possible pairs of cloud clusters larger than 5000 km^2, in frames adjacent in time, was calculated. If the area of overlap exceeded 10^4 km^2, or if it exceeded 50% of the area of either of the cloud clusters, a match was declared, and those two cloud clusters were considered to be part of the same *time cluster.* These parameters are discussed and varied in section 7. For each of the resulting time clusters, some bulk statistics were cal-

culated: the times and centroids of the start and end points, the time and centroid of the time cluster at its time of maximum size, and the total cold cloud coverage (area × time) of the time cluster.

4. Cluster size distributions

The vast majority of cloud clusters as defined above are tiny, many consisting of just one pixel (single clouds rather than true clusters). Previous studies have found that cluster sizes, like many other parameters describing atmospheric convective clouds, are nearly lognormally distributed (Williams and Houze 1987; Lòpez 1977). Figure 3 shows the size distributions of 208- and 198-K cloud clusters. The ordinate is accumulated frequency plotted on a scale that is the accumulated normal distribution, while the abscissa is size (km^2) on a logarithmic scale. On such a graph, a lognormally distributed variable appears as a straight line. Figure 3 indicates that 50% of cloud clusters are smaller than 300 km^2, while 90% are smaller than 4500 km^2, etc.

Deviation from lognormality is observed in both the lower and upper tails of the distribution. Such deviation indicates a truncated lognormal distribution, characteristic of a variable that has natural limits (Lòpez 1977). The size at which the distribution deviates from lognormal is approximately 10^5 km^2, indicating a linear dimension of approximately 300 km. This important size scale is approximately the horizontal distance

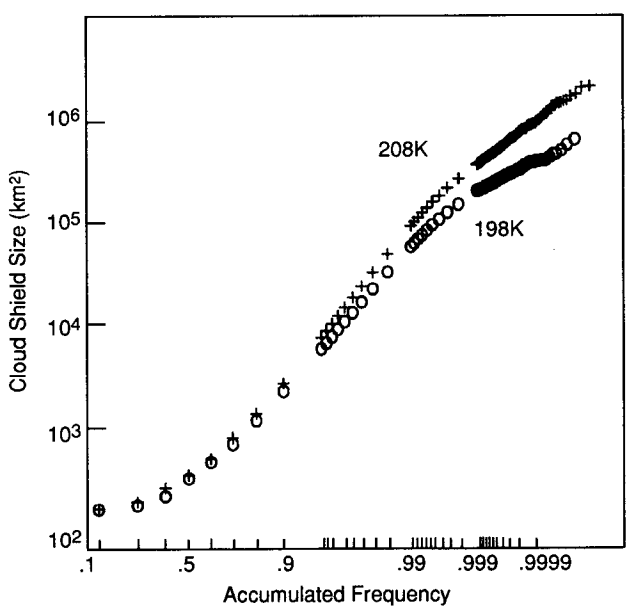

FIG. 3. Lognormal test for cloud-cluster size distributions. Cumulative frequency (number fraction) on an accumulated normal distribution scale versus cluster size on a logarithmic scale. If cloud-cluster sizes were lognormally distributed, the plot would be a straight line.

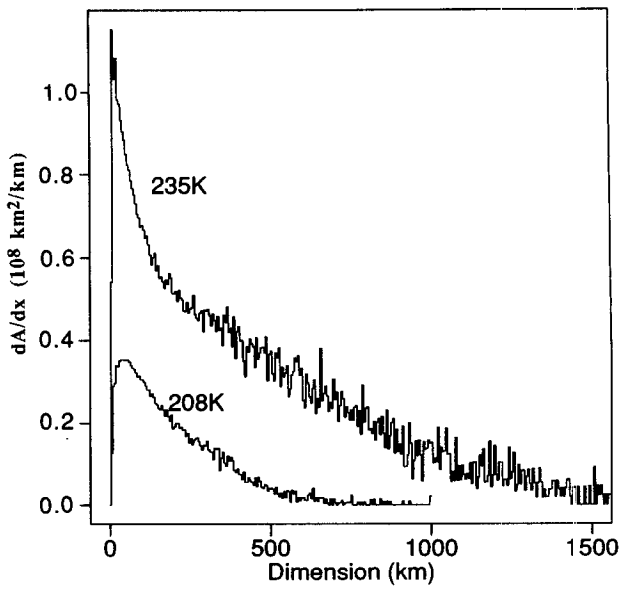

FIG. 4. Cold cloud area dA/dx as a function of cloud-cluster size x, where A is the total sampled cold cloud area (in all images) and x is a linear size measure [$(\text{area})^{1/2}$] for each cloud cluster.

that ice particles can travel from their convective-cell sources before falling out. The deviation from lognormality at small size occurs near 250 km^2, almost at the resolution limit of the data. However, the aspect ratio for deep penetrative convection is near unity at a minimum, so even a single cumulonimbus reaching the 208-K level (approximately 14-km altitude) should make a cold anvil larger than one 10-km pixel. It is therefore likely that deviation from the lognormal model at small sizes would be observed even with data at finer spatial resolution.

Number distributions are not very revealing about the relative importance of clusters of various sizes. The number of clusters per unit size interval (dN/dS) versus size S (km^2) are completely dominated by the smallest clusters. In a plot of cloud cover per unit size interval ($dA/dS = SdN/dS$), the size intervals at small S still dominate the distribution [e.g., Fig. 15 of Williams and Houze (1987), but note that they discarded all clusters smaller than 5000 km^2]. Figure 4 shows instead dA/dx versus x, where $x = S^{1/2}$. Area under the curve is proportional to cloudiness, but the size intervals at large S have been compressed together into fewer x intervals, bringing up the curve at the large-size end of the distribution.

No significant mesoscale peaks are evident in the distributions of either 208- or 235-K clusters; the distributions slope off smoothly with increasing size. Machado et al. (1992) have presented similar size distributions of cold cloud coverage as a function of a linear measure (like x) of cloud-cluster size, for Atlantic and

African cloud clusters (their Fig. 3). However, their logarithmic abscissa compresses the structure of the peak, while their logarithmic ordinate greatly deemphasizes the long tail of the distribution toward large sizes. The area under their curves is not proportional to cloud coverage.

Figure 5 shows cumulative fractional area coverage with increasing cluster size, the normalized cumulative sum of the distribution shown in Fig. 4. The dashed horizontal lines divide the size distribution into size quartiles, each quartile contributing an equal amount to the total area of cloud top colder than the indicated temperature. Figure 5 shows that, despite the lack of any mesoscale peak in the size distributions, mesoscale clusters are important contributors to total cloudiness and, by implication, rainfall. Half of the 208-K cloudiness is in clusters larger than 2×10^4 km^2, while half the 235-K cloudiness is in clusters larger than 10^5 km^2. The small, medium, large, and giant size ranges used to subdivide temperature histograms within 235-K clusters (section 2; Figs. 11–12) were selected on the basis of the size quartiles for a small subset of the cloud clusters over the western Pacific in 1986/87. It is clear from Fig. 5 that "giant" 235-K clusters (>640 000 km^2) do not usually account for as much of the moderately cold cloud as they did over the west Pacific during the 1986/87 El Niño.

Another structural parameter of interest is the perimeter of each cloud cluster. Figure 6 shows a log–log plot of perimeter versus (area)$^{1/2}$ for the −38°C cloud clusters. The slope of the fitted line, which corresponds to the fractal dimension[3] of the perimeters, is 1.4, in agreement with the 1.4–1.5 range quoted by Cahalan and Joseph (1989) for their ITCZ deep convective clouds. The linear fit is not especially good: the larger clusters are increasingly ragged, with very long perimeters for their area.

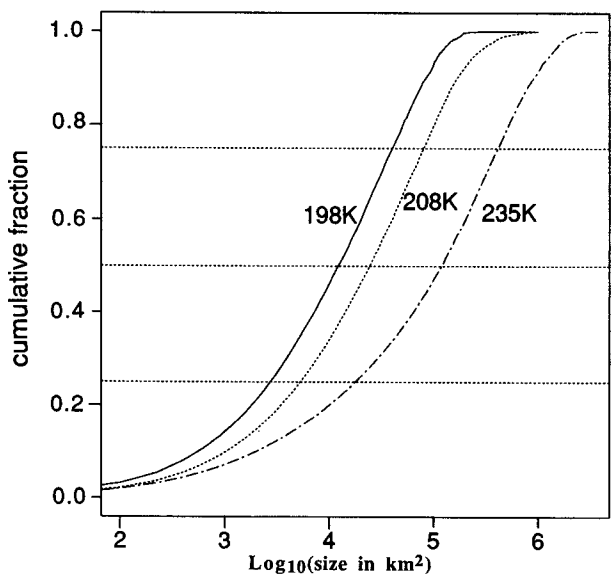

FIG. 5. Fraction of the total sampled cold cloud area that is accounted for by cloud clusters up to the indicated size. The dashed horizontal lines divide the size distribution into size quartiles, each quartile contributing an equal amount to the total area of cloud top colder than the indicated temperature.

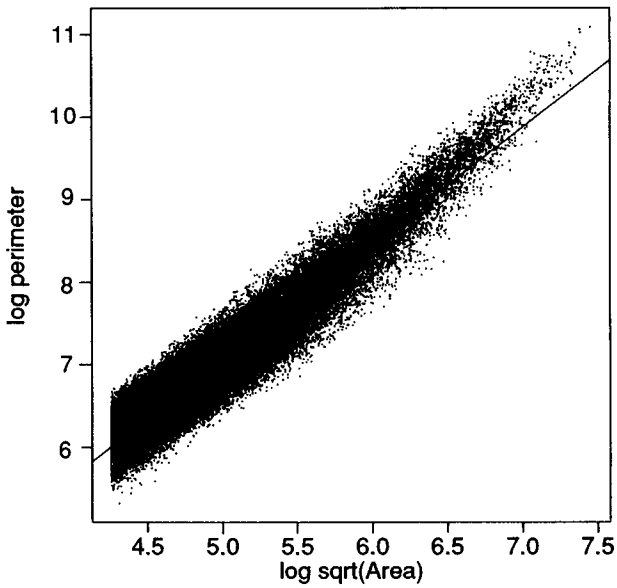

FIG. 6. Perimeter versus (area)$^{1/2}$ for the 235-K cloud clusters. The ordinate is the log of the square root of the cloud-cluster size (km), and the abscissa is the log of the perimeter length (km). The fitted line has a slope of 1.4, the "fractal dimension."

5. The diurnal cycle

The diurnal cycle of deep convection over the tropical oceans is a surprisingly rich and subtle question. In recent years the question has been taken up by Gray and Jacobson (1977), Houze et al. (1981), Albright et al. (1985), and Randall et al. (1991). There are a few situations in which the diurnal cycle is strong and easy to understand. For example, maps of the incidence of small (1000–3000 km^2) very cold cloud clusters in the morning and afternoon need no geographical overlay (Fig. 7). The small, short-lived convective clouds shown in Fig. 7 occur over the large islands of the maritime continent during the afternoon, and over the surrounding seas during the night and morning.

Similar maps of the incidence of large (>30 000

[3] The *fractal dimension* is a measure of the raggedness of the perimeter, and must lie between 1 and 2. Euclidean geometric shapes have a perimeter fractal dimension of 1 (Cahalan and Joseph 1989).

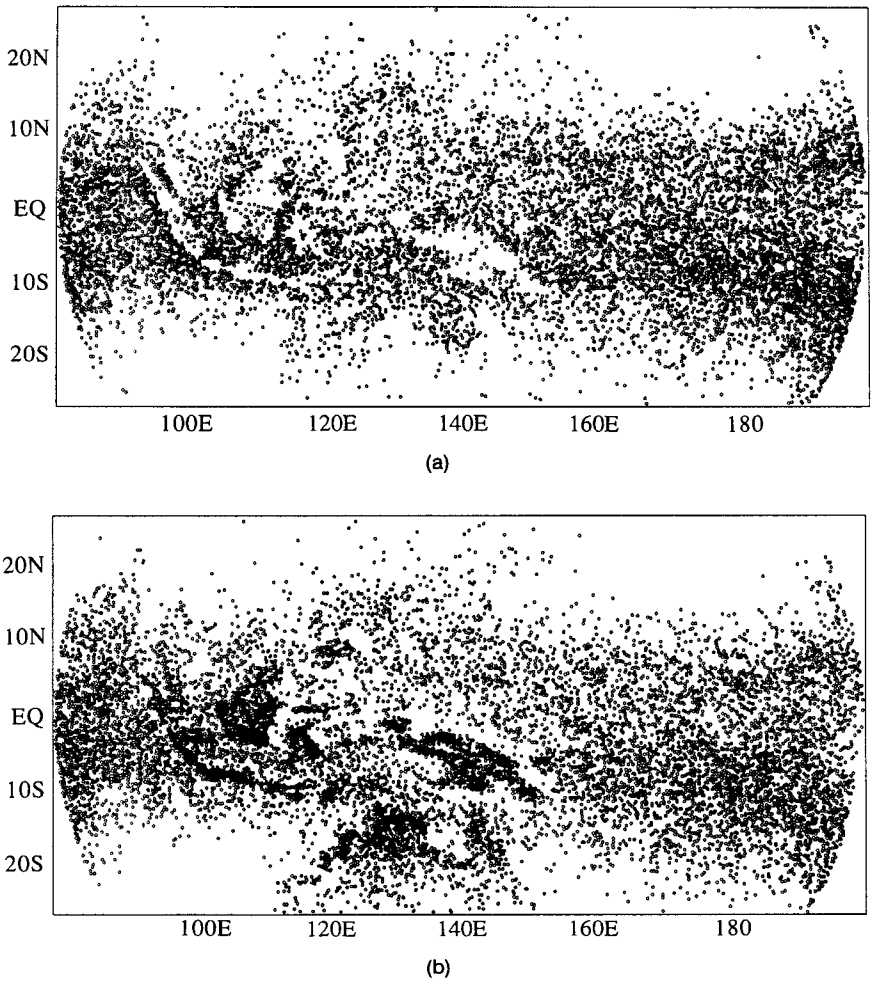

FIG. 7. Maps of all very cold (<208 K) cloud clusters 1000–3000 km^2 in area observed in images at (a) 2300 UTC (0900 LST at subsatellite point) and (b) 0800 UTC (1800 LST at subsatellite point).

km^2) very cold (208 K) cloud clusters, at the minimum and maximum of their diurnal cycle, do not show the geography quite so clearly (Fig. 8). Instead, a pronounced diurnal variation in the *total number* of large clusters is apparent, even over the open ocean, with numerous clusters observed during early morning and fewer in the evening hours. The diurnal cycle in the area covered by large clusters also peaks in the early morning, as shown in Fig. 9a. The largest-size quartile of 208-K cloud clusters (>65 000 km^2; dashed line 4 in Fig. 9a) is strongly diurnally modulated, with a dawn-to-dusk ratio of 2:1 or more. This large-cluster variation dominates and determines the overall diurnal cycle in very cold cloudiness. The diurnal cycle of moderately cold cloudiness (<235 K) is also dominated by the contribution from the largest clusters (Fig. 9b). But moderately cold cloud area has its peak in the afternoon. In other words, the diurnal cycle of cold cloudiness overturns with temperature. Short and Wallace (1980) reached a similar conclusion from twice-daily observations.

Figure 10 shows a contour plot of the diurnal cycle of the coverage of the TC region by cloud tops whose T_{BB} lay within 1°C intervals at the indicated temperatures. The units of the plotted field are percent of daily-mean 235-K coverage per degree (note, for example, that the values in the 40° range between −40° and −80°C average about 2.5%). This figure (very similar to Fig. 9 of Albright et al. 1985) indicates that the diurnal maximum in very cold cloudiness (less than −65°C) is before dawn, while warmer-topped cloudiness (near −40°C) peaks in the afternoon. The coverage by clouds with successively warmer tops peaks later and later in the afternoon. Albright et al. (1985) suggested that the afternoon peak represented a "second regime of less deep convection." They also ac-

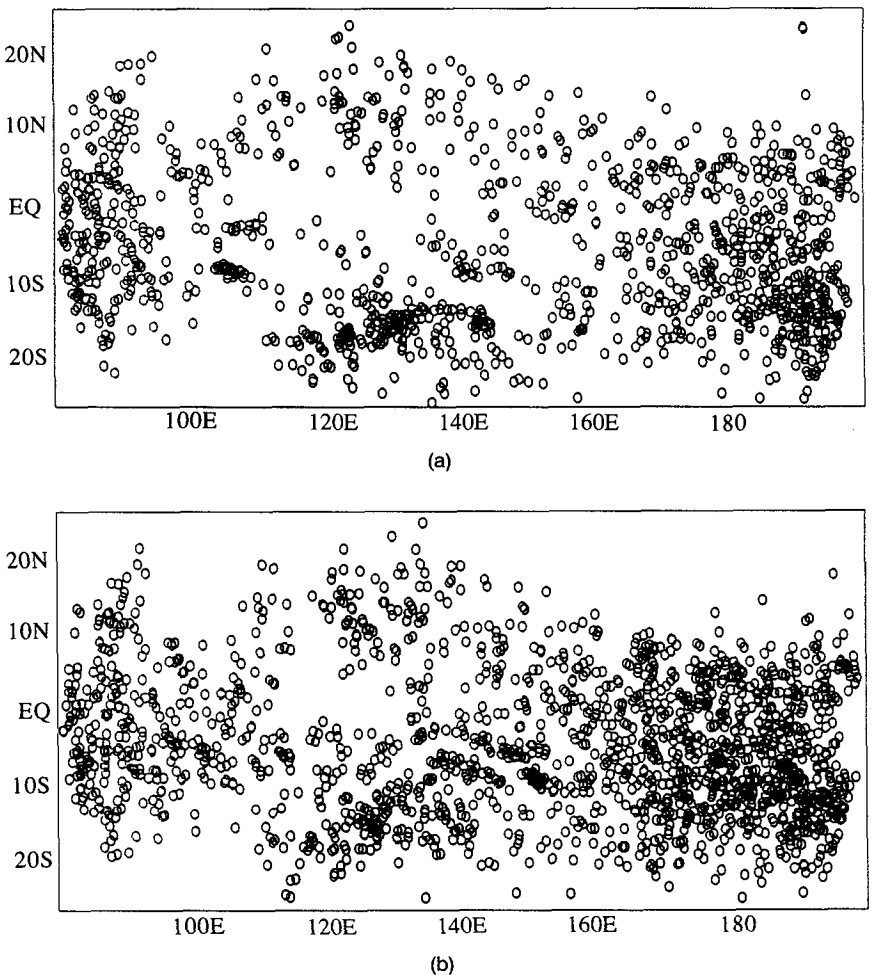

FIG. 8. Maps of all very cold (<208 K) cloud clusters greater than 30 000 km^2 in area observed in images at (a) 0800 UTC (1800 LST at subsatellite point) and (b) 1700 UTC (0300 LST at subsatellite point).

knowledged the possibility that it corresponded to the large nimbostratus portion of mesoscale convective systems, which develops from the deep convective portion after a time lag of a few hours.

Figure 11 shows similar contour plots of the TC diurnal cycle for temperatures colder than 235 K (corresponding to just the upper portion of Fig. 10), subdivided according to cloud cluster size (the size of the 235-K contour). The "small" size category shows little diurnal variation. It is instead the mesoscale clusters of larger sizes that contribute to the diurnal cycle, as their deep convection (very cold cloud) peaks before dawn and collapses around noon, followed by a rather sudden surge in moderately cold cloud top area in the afternoon. The phase of the diurnal cycle is similar in all size categories, but the amplitude increases with cluster size, even from the "large" ($2.5–6.4 \times 10^5$ km^2) to "giant" ($>6.4 \times 10^5$ km^2) categories.

Figure 12 shows similar contour plots for the MC geographical zone. Giant clusters constitute a smaller fraction of the total cloudiness in the MC region than in the other regions. But again, the early morning maximum in deep convection and afternoon surge in warmer cloud area is most strongly apparent in the large and giant clusters. In addition, a modest afternoon pulse in small clusters is apparent (cf. Figs. 11a, 12a), contributed by convective showers over the heated islands. Figure 13 shows the giant-cluster contour plots for the WP and IO regions, and indicates a diurnal cycle process similar to that in giant clusters elsewhere. Some evidence of a second peak in moderately cold cloud before noon shows up in the MC and IO giant cluster plots. However, a substantial correction has been applied to account for the 70 (out of 281) days on which the subsatellite noon (0200 UTC) picture was missing, so fine structure near midday may simply

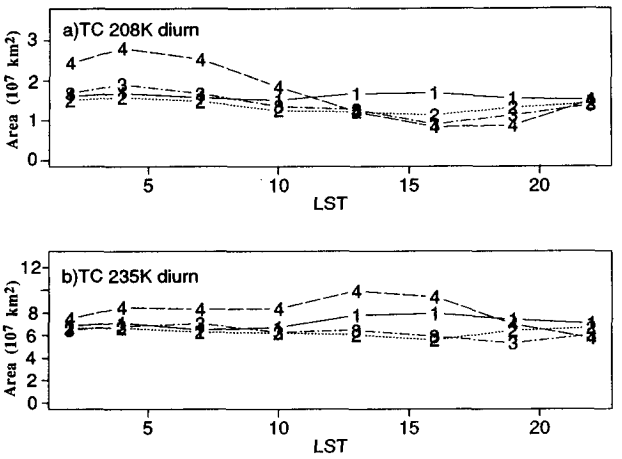

FIG. 9. Diurnal cycle of cold cloud area observed within the TC domain, subdivided into cloud cluster-size quartiles (1 = smallest, 4 = largest). (a) Very cold (<208 K) cloudiness; (b) moderately cold (<235 K) cloudiness.

represent the different sampling of cloudiness at the different synoptic hours.

This size dependence indicates that *the diurnal cycle of cold-topped cloudiness is a sun-synchronous life-cycle process in large mesoscale cloud clusters, not a diurnal modulation of cumulus or cumulonimbus clouds.* The cloud clusters apparently slump down vertically and spread out horizontally (e.g., Lilly 1988) following the collapse of their deep convection after sunrise. But why do the deep convective parts of these mesoscale systems preferentially grow during the night and fail to grow or even persist during the day? Explanations are of essentially two types: direct effects of solar radiation on the thermal stratification, and the effects of radiation-induced circulations.

Gray and Jacobson (1977) found that heavy-rain events in the western Pacific contribute most of their rainfall in the early morning hours, while lighter rain events deliver rain throughout the day. They inferred that the *heavier rain* events corresponded to *spatially larger* organized mesoscale systems. They offered the explanation that mesoscale pressure gradients, forced by differences in the radiative heating rate between clear and cloudy columns of the atmosphere, create mesoscale circulations that favor upward motion in the cloudy columns in the early morning. This mechanism was postulated to operate only in systems with lifetimes comparable to a day.

But although the vertical circulation in MCSs includes deep upward motion, it is clear from elementary thermodynamic arguments that the incidence of deep convection depends primarily on processes that lift boundary-layer air to its level of free convection (e.g., Ooyama 1971; Mapes and Houze 1992). Once this lifting takes place, the rest of the deep ascent is simply an inevitable consequence of conditional instability. It is not immediately obvious how the deep, diffuse radiatively driven vertical circulation postulated by Gray and Jacobsen (1977) affects the intense, localized low-level processes controlling the development of new convective cells.

Randall et al. (1991) concluded, from a study of the output of a general circulation model with parameterized convection, that "stabilization due to absorption of solar radiation, primarily by clouds, tends to suppress convection during the afternoon, relative to the period before sunrise, to such an extent that *this mechanism alone can qualitatively account for the observed diurnal cycle of precipitation over the oceans.*" But again, it remains unclear exactly how the primarily upper-tropospheric solar warming shown by Randall et al. (1991) impacts the low-level processes involved in the development of real convection. Furthermore, such an explanation does not address the cluster-size dependence of the diurnal cycle.

In summary, the physical processes that cause the observed cluster-size-dependent diurnal cycle of tropical convection remain substantially unexplained.

6. The intraseasonal variation (ISV)

The ISV (Nakazawa 1988) is an eastward-moving envelope of enhanced convective cloudiness that crosses the field of view of the GMS in about 30 days. Intraseasonal variability in the tropics has also been

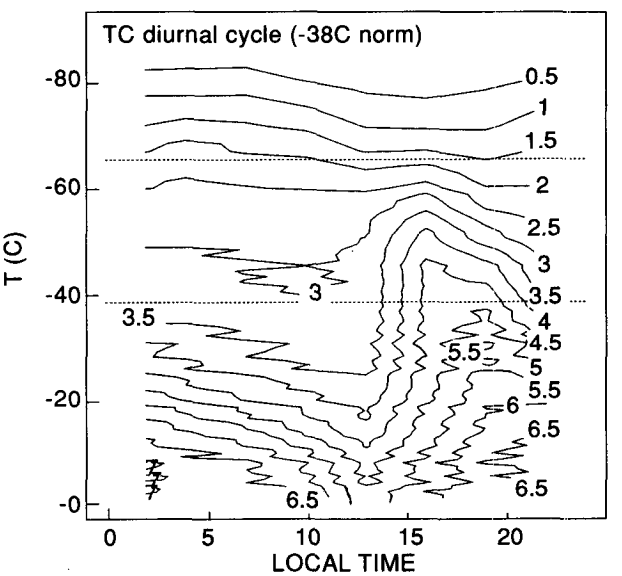

FIG. 10. Percentage of the daily mean moderately cold (<235 K) cloud area, within 1°C temperature intervals at the indicated temperatures, as a function of local time of day, in the TC geographical domain. For reference, 208 and 235 K are indicated with dashed lines.

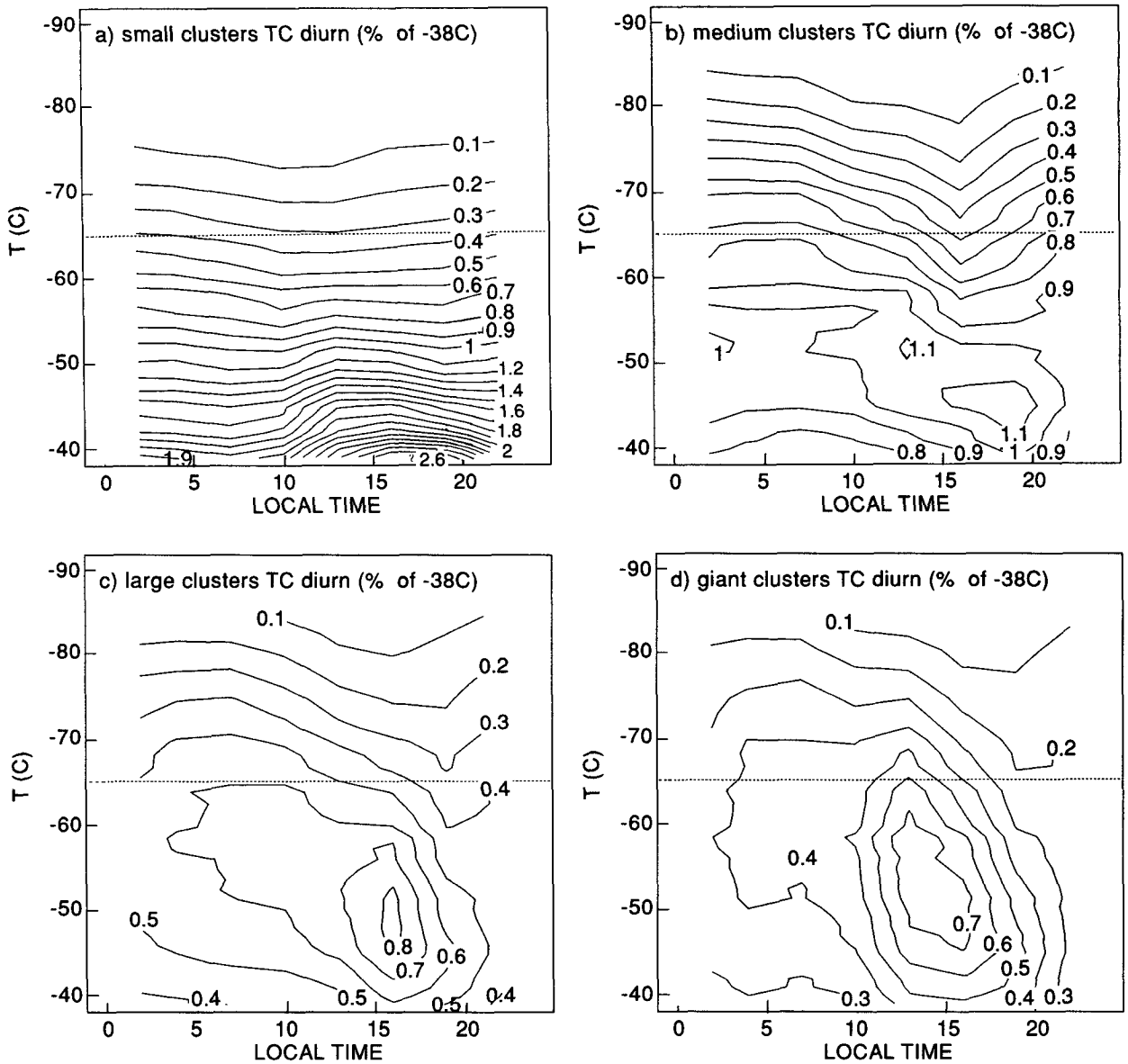

FIG. 11. As in Fig. 10 but subdivided according to moderately cold (<235 K) cloud-cluster size. Vertical scale differs from Fig. 10, because only temperatures colder than 235 K lie within the 235-K cloud clusters.

identified in pressure, OLR, velocity potential, and Indian rainfall (Madden and Julian 1972; Knutson and Weickmann 1987; Hartmann and Michelsen 1989).

Figure 14 shows time–longitude plots of all 208-K cloud clusters observed during the 1986/87 season within the entire tropical latitude belt, in three size ranges. The three size ranges represent comparable fractions of the total 208-K cloud cover, and the plotting characters have been scaled so that a similar amount of ink appears in each panel. Westward-moving tropical cyclones and other individual cloud clusters are clearly evident. An eastward-moving intraseasonal envelope modulating the cloudiness can also be detected (especially after a peek at Fig. 15a).

This intraseasonal variation may be quantified. Figure 15 shows weekly mean values of percent high cloudiness (PHC_{228}, the area and time fractional coverage by cloud top colder than 228 K) in each of ten longitude bins. Each bin is a rectangle on the GMS imagery, 100 pixels wide, and extends from 15°S to 15°N at the subsatellite longitude. Two eastward-moving cloudiness enhancements are apparent in each of

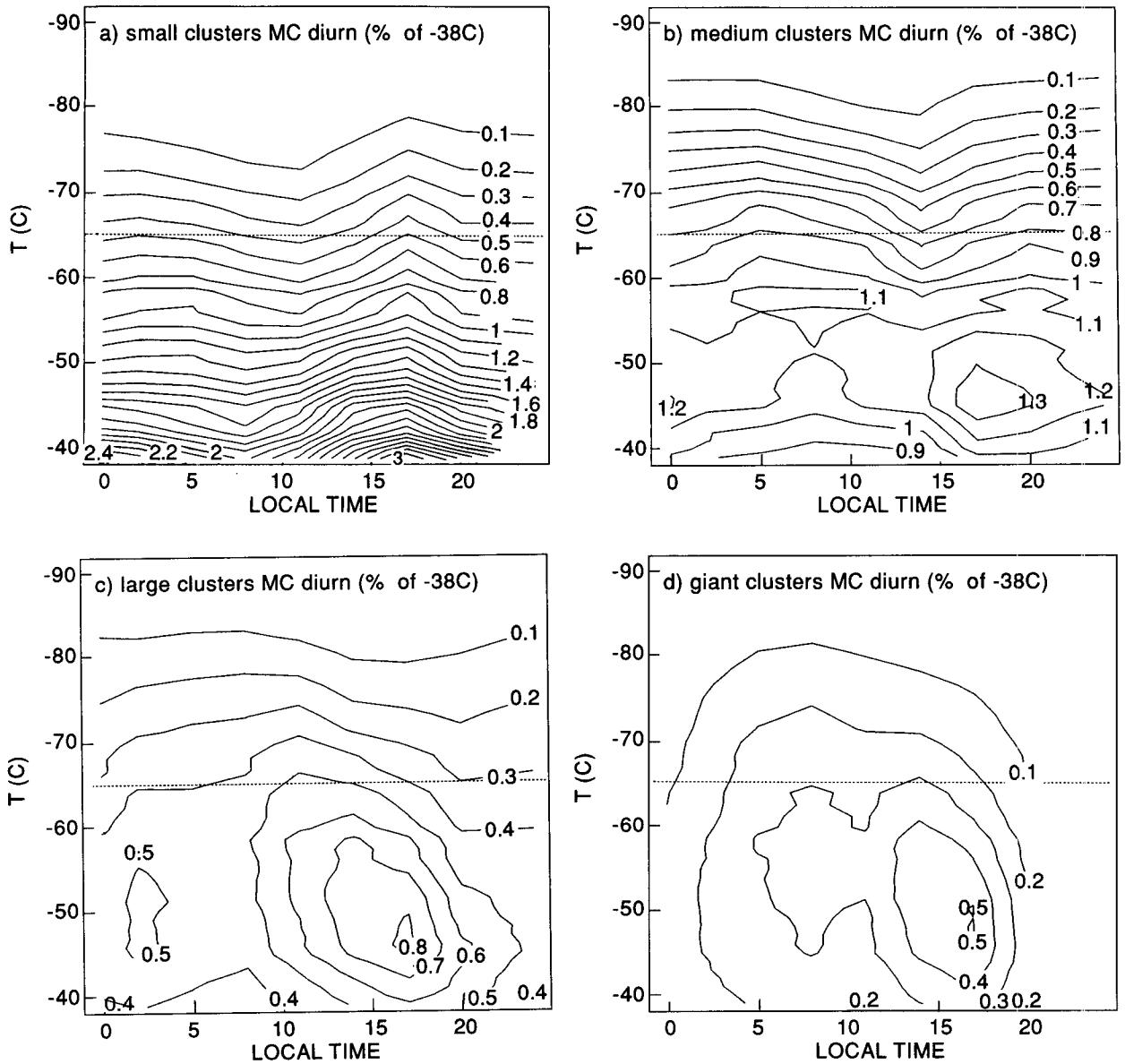

FIG. 12. As in Fig. 11 but for the MC geographical domain.

the three years. The 10% contour of PHC_{228} at this resolution makes an adequate threshold for defining the ISV. Composite categories have been defined as shown on Fig. 15, with the ISV divided into "enhanced" and "suppressed" weeks in both the MC and TC regions.

Cloud-cluster size distributions for ISV enhanced and suppressed conditions are shown in Figs. 16–18. Figure 16 shows very cold (less than −65°C) cloudiness. The enhanced conditions have more area covered by cloud in all size categories. But if the curves are normalized so that the peaks match (Fig. 17), it becomes clearer that *the intraseasonal variation modulates large clusters proportionately more than small clusters.* Similar plots for the 235-K clusters (with small sizes excluded for computational reasons) show that, at that temperature threshold also, the ISV modulates all size categories but modulates the large categories proportionately more.

7. Time clusters and superclusters

The cloud clusters within each individual frame of the satellite imagery were matched with clusters in the

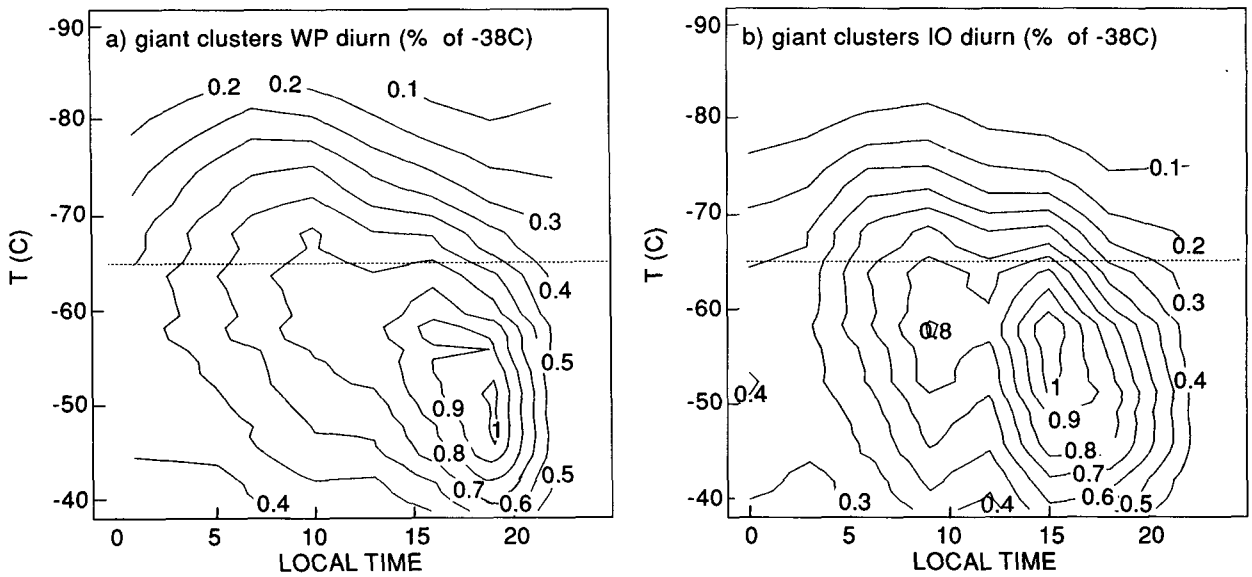

FIG. 13. As in Fig. 11 but giant clusters only for WP and IO geographical domains.

following frame, according to the rules described in section 3 (overlap area exceeding 50% of a 208-K cluster or 10 000 km^2; only clusters greater than 5000 km^2 considered), to yield *time clusters*. Time clusters may consist (in any given frame) of several cloud clusters if those clusters have split from a common mother cluster in a previous frame or are destined to merge in some later frame (illustrated in Fig. 2 of Williams and Houze 1987). The cluster-matching technique, and its sensitivity to the parameters above, is best illustrated with an example.

Multiscale structure of west Pacific convective cloudiness has been explored by Nakazawa (1988), Lau et al. (1991), and Sui and Lau (1992). In Nakazawa's famous example from November 1986, reprinted in Fig. 19, an eastward-moving "supercluster" contains several westward-moving cloud clusters. An alternative presentation of this same data directly in terms of cloud clusters is shown in Fig. 20. Figure 20 is a temporal, longitudinal, and latitudinal subset of the plots in Fig. 14, but with all clusters larger than 5000 km^2 indicated. The individual cloud clusters do indeed move westward within an eastward-moving envelope. It is our impression from viewing the data in time lapse that cloud clusters all over the Pacific were moving westward.

The time clusters observed during November 1986 are plotted in the same time–longitude coordinates in Fig. 21. An arrow is plotted from the position (centroid) of each time cluster in its first frame to its position in its last frame. An oval is plotted at the position of each time cluster at its time of maximum size. The oval's size (area on the page) is proportional to the total (area × time) cold cloud coverage associated with the time cluster. Only time clusters within the 5°S–5°N latitude strip at their time of maximum size are plotted, and nothing is plotted for time clusters appearing in only one frame.

Figure 21a shows the time clusters when the program is run with the parameters indicated above [identical to those used in Williams and Houze (1987) except for our colder −65°C threshold]. The technique has no difficulty finding the westward-moving clusters in early November. In late November, however, the cloud clusters begin to overlap so much that almost all of the 208-K cloudiness gets subsumed into a single eastward-moving week-long[4] time cluster, which, because it lasts longer than two days, we will call a *supercluster*. The late stages of this supercluster included twin cyclones straddling the equator.

A more stringent set of parameters could be used to define time clusters, in order to break up the late November supercluster. Figure 21b shows the time clusters found when the minimum size of 208-K cloud clusters considered in the time-matching process is raised to 25 000 km^2. Many of the early November clusters get missed, but still a giant multiday time cluster dominates the picture in late November. Figure 21c shows the time clusters found when the temperature threshold is decreased to 198 K (−75°C). The late November cloudiness is resolved into three main time clusters of slightly less than two days' duration each. However, a

[4] Three consecutive frames of data from 22 November were missing.

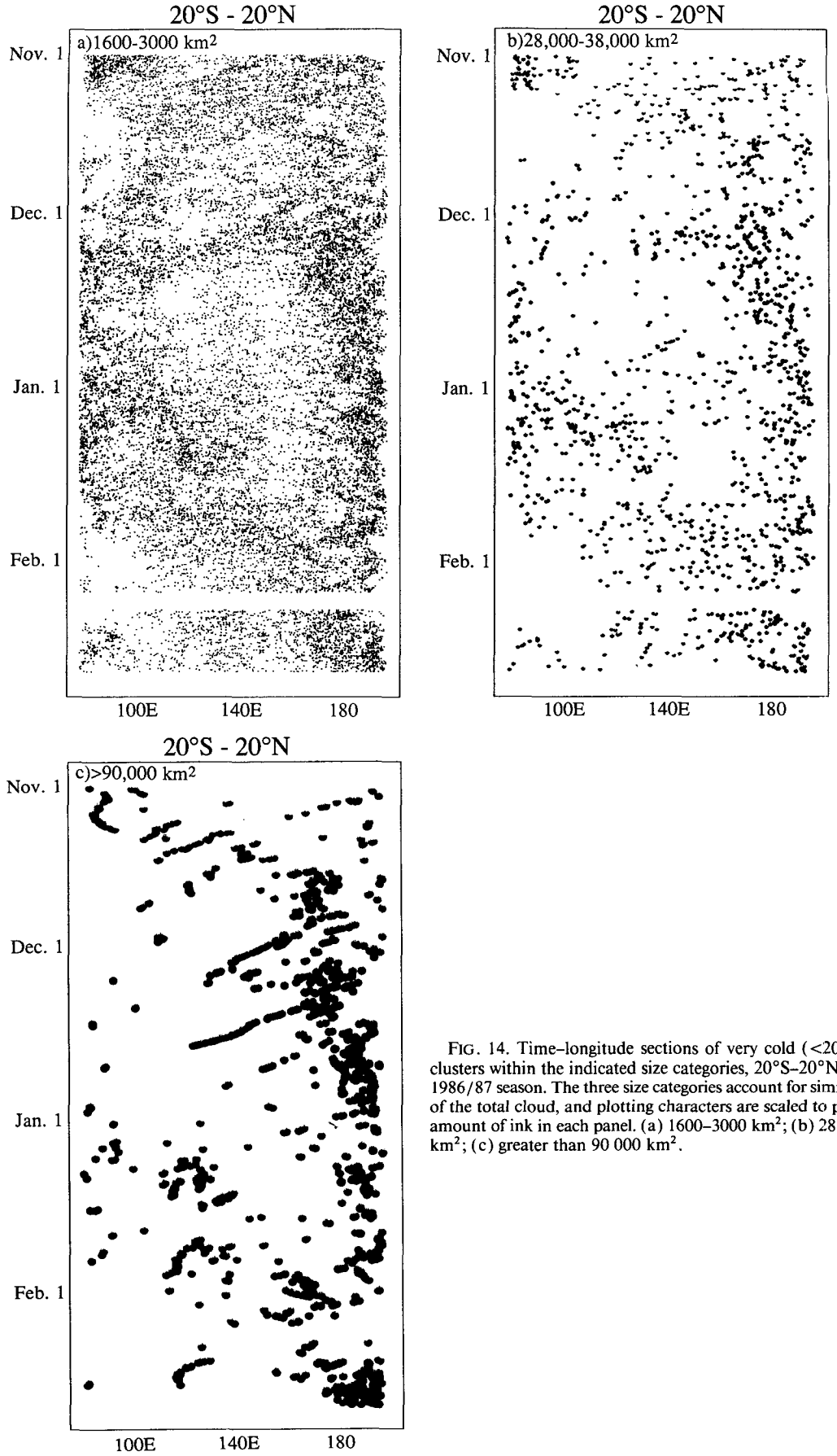

FIG. 14. Time–longitude sections of very cold (<208 K) cloud clusters within the indicated size categories, 20°S–20°N, during the 1986/87 season. The three size categories account for similar fractions of the total cloud, and plotting characters are scaled to put a similar amount of ink in each panel. (a) 1600–3000 km^2; (b) 28 000–38 000 km^2; (c) greater than 90 000 km^2.

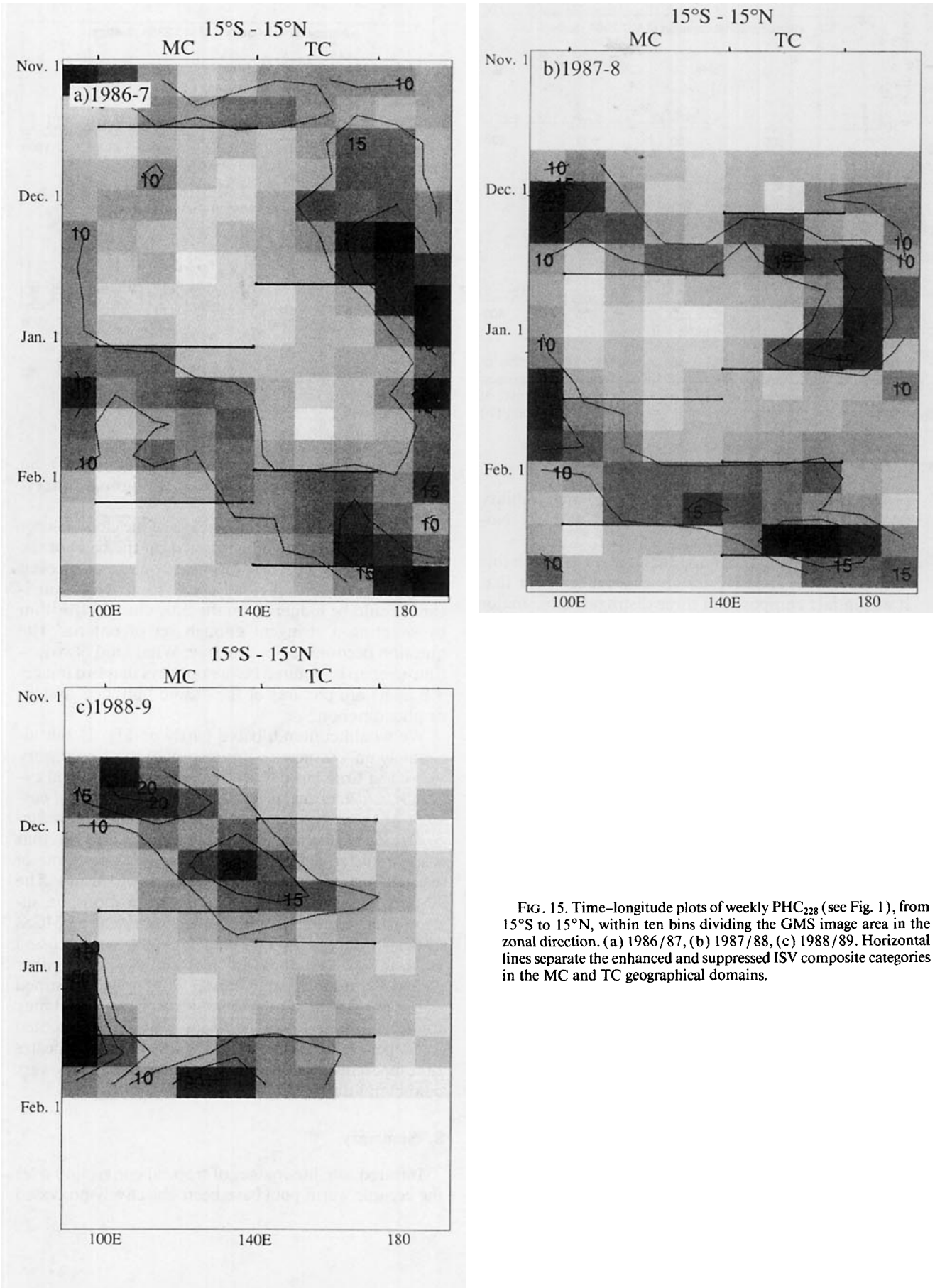

FIG. 15. Time–longitude plots of weekly PHC_{228} (see Fig. 1), from 15°S to 15°N, within ten bins dividing the GMS image area in the zonal direction. (a) 1986/87, (b) 1987/88, (c) 1988/89. Horizontal lines separate the enhanced and suppressed ISV composite categories in the MC and TC geographical domains.

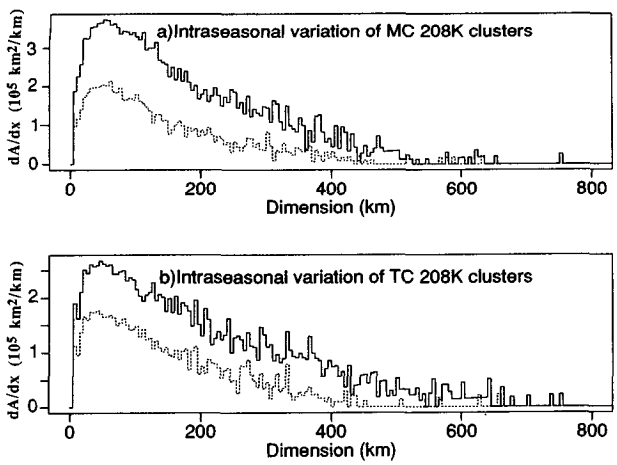

FIG. 16. Very cold (<208 K) cloud area dA/dx as a function of cloud cluster size x (see Fig. 4), for enhanced (solid) and suppressed (dotted) ISV composite categories. Units are in kilometers square of observed cloud per unit x interval per week. (a) MC domain; (b) TC domain.

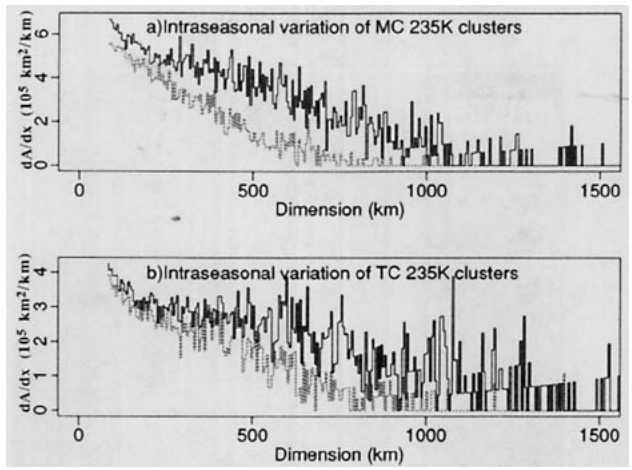

FIG. 18. As in Fig. 16 but for moderately cold (<235 K) cloud clusters.

price has been paid in terms of the technique's ability to resolve the ordinary cloud clusters of early November.

A careful look at the individual images in which this late November supercluster appears makes clear that it was in fact composed of three distinguishable major convective subevents, as found by the 198-K time cluster analysis. However, there are examples of multiday superclustering even at 198 K. The largest supercluster we have found ran from 0500 UTC 22 February 1987 through 2000 UTC 28 February 1987, the end of our 1987 dataset. Another 198-K supercluster was apparent from 14 to 17 January 1987 as (noncyclone) convection in the 1987 Australian monsoon (studied in AMEX and EMEX, e.g., Mapes and Houze 1992). So even the 198-K threshold does not eliminate superclustering.

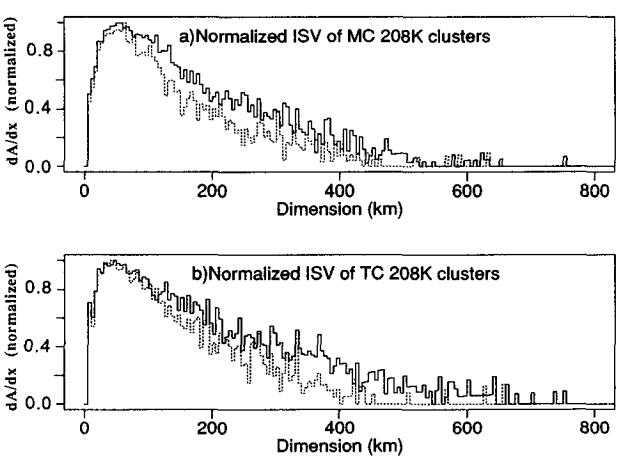

FIG. 17. Normalized versions of the distribution functions in Fig. 16.

It is apparent that the parameters of the cloud-cluster tracking program must be selected on the basis of the desired output. The real physical continuity of even the most persistent of cloud clusters (such as a hurricane) could be hidden from the time cluster algorithm by selecting a stringent enough set of criteria. The question becomes a physical one: What kind of space–time overlap is required before one says that two images 3 h apart are pictures of the "same" physical system or phenomenon?

We would contend, based partly on Fig. 21 but ultimately on a subjective impression of the 3-h imagery viewed in time lapse that, even excluding tropical cyclones, *superclusters are a physical reality: it is not possible or meaningful to separate them into individual cloud clusters lasting less than two days.* Note also that a supercluster generally consists, in any one frame of satellite imagery, of several distinct cloud clusters. The EMEX flights into the 1987 Australian monsoon superclusters always found distinct, well-defined MCSs corresponding to the very cold cloud tops, as discussed in section 2. But those distinct cloud clusters either shared a common parent cluster with, or were destined to merge with, their neighbors. A mechanism that may underlie this gregarious behavior of MCSs is presented in Mapes (1993). Figure 7 of Mapes (1993) indicates that superclusters accounted for almost half of the very cold cloud during January–February 1987.

8. Summary

Infrared satellite images of tropical convection over the oceanic warm pool have been objectively processed

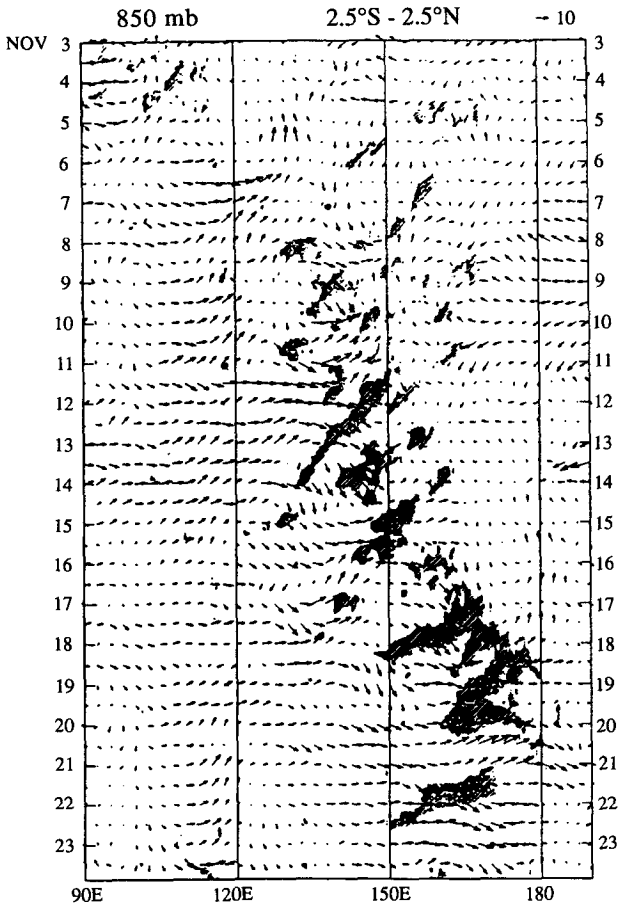

FIG. 19. Time–longitude section of a cold cloudiness index (shaded) and 850-mb wind in the latitude swath 2.5°S–2.5°N, 3 November 1986 to 24 November 1986. (From Fig. 11 of Nakazawa 1988).

to reveal "cloud clusters," connected areas with cloud-top temperatures lower than a given threshold value. Results in this paper are for a very cold threshold (208 K or −65°C), corresponding roughly to the radar echo area within Australian monsoon cloud clusters, and a moderately cold threshold (235 K or −38°C) frequently used in climatic rainfall estimation. Cloud clusters span a somewhat lognormal distribution of sizes. No separate mesoscale peak is apparent in the distribution, but half the less than 208-K cloudiness is contributed by cloud clusters greater than 20 000 km^2 in size, while half the less than 235-K cloudiness is contributed by cloud clusters greater than 100 000 km^2 in size.

The diurnal cycle of cold cloudiness is primarily a sun-synchronous process within large and giant clusters, not a modulation of populations of cumulus or cumulonimbus clouds. Deep convection in these clusters (as inferred from very cold cloud) peaks before dawn, and decreases through the morning. Moderately cold cloud-top area increases suddenly in the afternoon, suggesting an outward surge that lags the collapse of the deep convection by a few hours. In the maritime continent, a small additional diurnal cycle is present, as a burst of small cloud clusters appears over the large islands in the afternoon (Fig. 7).

The eastward-propagating ISV is apparent in cold cloudiness integrated across the entire deep tropical latitude belt. The ISV modulates cloud clusters of all sizes, but larger clusters are proportionately more affected than smaller clusters.

Cloud clusters have been tracked in time to reveal "time clusters," which are sets of cloud clusters satisfying certain criteria about their spatial overlap from one frame of imagery to the next. In some cases, convection is so gregarious and interconnected that these time clusters last for days and consist of numerous separate cloud clusters within some individual frames. Time clusters exceeding two days in duration we call superclusters. While ordinary cloud clusters move by advection and propagation, these superclusters tend to move with their parent synoptic-scale circulations (they are stationary in the monsoon, or eastward-moving in the ISV, as seen in Fig. 21a). It is, of course, possible

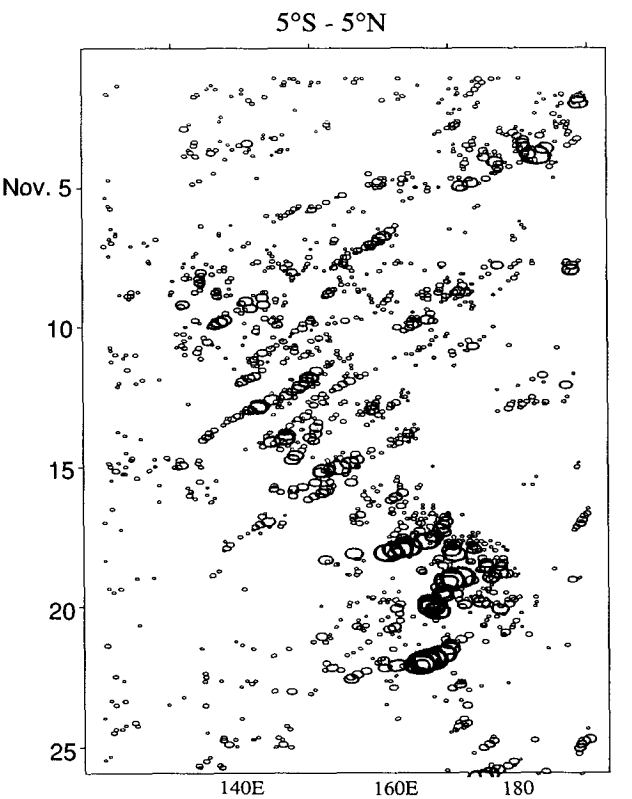

FIG. 20. Time–longitude section of very cold (<208 K) cloud clusters centered between 5°S and 5°N during November 1986. Compare to rightmost two-thirds of Fig. 19.

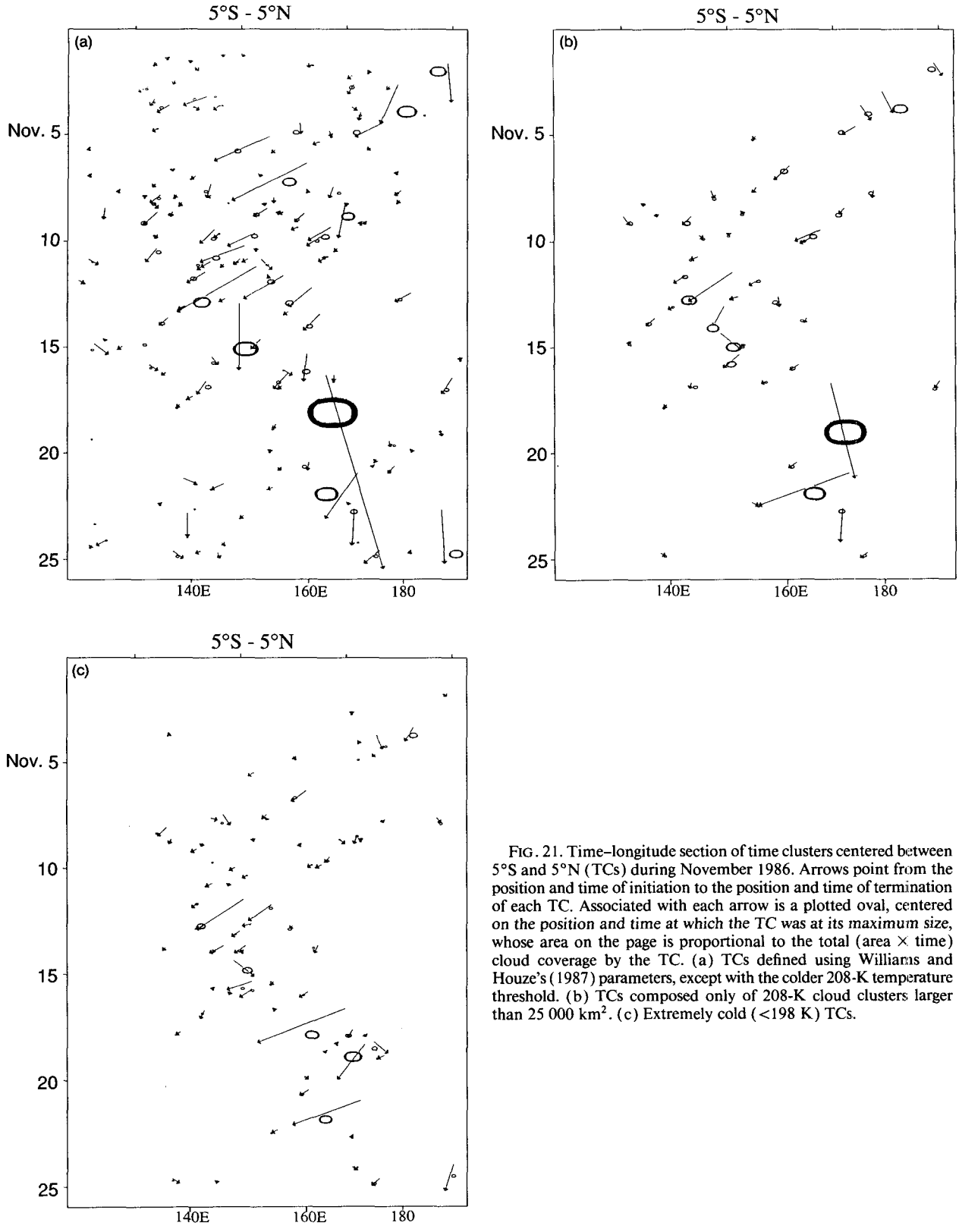

FIG. 21. Time–longitude section of time clusters centered between 5°S and 5°N (TCs) during November 1986. Arrows point from the position and time of initiation to the position and time of termination of each TC. Associated with each arrow is a plotted oval, centered on the position and time at which the TC was at its maximum size, whose area on the page is proportional to the total (area × time) cloud coverage by the TC. (a) TCs defined using Williams and Houze's (1987) parameters, except with the colder 208-K temperature threshold. (b) TCs composed only of 208-K cloud clusters larger than 25 000 km^2. (c) Extremely cold (<198 K) TCs.

to specify ever more stringent criteria and thereby eliminate superclusters, but only at the cost of losing the ability to track any time clusters at all. Although they may exist at a given time as several distinct cloud clusters, these superclusters are apparently real physical entities, with actual space–time continuity of very cold-topped cloud and possibly precipitation areas.

Acknowledgments. Special thanks to Stefan Lüthi for his work on this project and to G. C. Gudmundson for editing the manuscript. This research was supported by the U.S. National Atmospheric and Oceanic Administration's Hurricane Research Division and the National Science Foundation under NSF Grants ATM9008406 and ATM9024431, and by the U.S. National Aeronautics and Space Administration Grants NAG51599 and NAGW2633.

REFERENCES

Albright, M. D., E. E. Recker, R. J. Reed, and R. Dang, 1985: The diurnal variation of deep convection in the central tropical Pacific during January–February 1979. *Mon. Wea. Rev.*, **113,** 1663–1680.

Arkin, P. A., 1979: The relationship between fractional coverage of high cloud and rainfall accumulations during GATE over the B-scale array. *Mon. Wea. Rev.*, **107,** 1382–1387.

——, and B. N. Meisner, 1987: The relationship between large-scale convective rainfall and cold cloud over the western hemisphere during 1982–1984. *Mon. Wea. Rev.*, **115,** 51–74.

Cahalan, R. F., and J. H. Joseph, 1989: Fractal statistics of cloud fields. *Mon. Wea. Rev.*, **117,** 261–272.

Chang, C.-P., 1970: Westward propagating cloud patterns in the tropical Pacific as seen from time composite satellite photographs. *J. Atmos. Sci.*, **27,** 133–138.

Fu, R., A. D. Del Genio, and W. B. Rossow, 1990: Behavior of deep convective clouds in the tropical Pacific deduced from ISCCP radiances. *J. Climate,* **3,** 1129–1152.

Gray, W. M., and R. W. Jacobson, 1977: Diurnal variation of deep cumulus convection. *Mon. Wea. Rev.*, **105,** 1171–1188.

Hartmann, D. L., and M. L. Michelsen, 1989: Intraseasonal periodicities in Indian rainfall. *J. Atmos. Sci.*, **46,** 2838–2862.

Houze, R. A., S. G. Geotis, F. D. Marks, and A. K. West, 1981: Winter monsoon convection in the vicinity of north Borneo. Part I: Structure and time variation of the clouds and precipitation. *Mon. Wea. Rev.*, **109,** 1595–1614.

Janowiak, J. E., and P. A. Arkin, 1991: Rainfall variations in the tropics during 1986–1989, as estimated from observations of cloud-top temperature. *J. Geophys. Res.*, **96,** 3359–3374.

Keenan, T. D., J. McBride, G. Holland, N. Davidson, and B. Gunn, 1989: Diurnal variations during the Australian Monsoon Experiment (AMEX) Phase II. *Mon. Wea. Rev.*, **117,** 2535–2552.

Knutson, T. R., and K. M. Weickmann, 1987: 30–60 day atmospheric oscillations: Composite life cycles of convection and circulation anomalies. *Mon. Wea. Rev.*, **115,** 1407–1436.

Lau, K. M., T. Nakazawa, and C.-H. Sui, 1991: Observations of cloud cluster hierarchies over the tropical western Pacific. *J. Geophys. Res.*, **96,** 3197–3208.

Leary, C. A., and R. A. Houze, Jr., 1979: The structure and evolution of convection in a tropical cloud cluster. *J. Atmos. Sci.*, **36,** 437–457.

Lilly, D. K., 1988: Cirrus outflow dynamics. *J. Atmos. Sci.*, **45,** 1594–1605.

Lòpez, R. E., 1977: The lognormal distribution and cumulus cloud populations. *Mon. Wea. Rev.*, **105,** 865–880.

Machado, L. A. T., M. Desbois, and J.-P. Duvel, 1992: Structural characteristics of deep convective systems over tropical Africa and the Atlantic Ocean. *Mon. Wea. Rev.*, **120,** 392–406.

Madden, R. A., and P. R. Julian, 1972: Description of global-scale circulation cells in the tropics with a 40–50 day period. *J. Atmos. Sci.*, **29,** 1109–1123.

Maddox, R. A., 1980: Mesoscale convective complexes. *Bull. Amer. Meteor. Soc.*, **61,** 1374–1387.

Mapes, B. E., 1993: Gregarious tropical convection. *J. Atmos. Sci.*, in press.

——, and R. A. Houze, Jr., 1992: An integrated view of the 1987 Australian monsoon and its mesoscale convective systems. Part I: Horizontal structure. *Q. J. Roy. Meteor. Soc.*, **118,** 927–663.

Miller, D., and J. M. Fritsch, 1991: Mesoscale convective complexes in the western Pacific region. *Mon. Wea. Rev.*, **119,** 2978–2992.

Nakazawa, T., 1988: Tropical superclusters within intraseasonal variations over the western Pacific. *J. Meteor. Soc. Japan,* **66,** 823–839.

Ooyama, K., 1971: A theory on parameterization of cumulus convection. *J. Meteor. Soc. Japan,* **49,** 744–756.

Randall, D. A., Harshvardan, and D. A. Dazlich, 1991: Diurnal variability of the hydrologic cycle in a general circulation model. *J. Atmos. Sci.*, **48,** 40–62.

Richards, F., and P. A. Arkin, 1981: On the relationship between satellite-observed cloud cover and precipitation. *Mon. Wea. Rev.*, **109,** 1081–1093.

Short, D. A., and J. M. Wallace, 1980: Satellite-inferred morning-to-evening cloudiness changes. *Mon. Wea. Rev.*, **108,** 1160–1169.

Sui, C.-H., and K.-M. Lau, 1992: Multiscale phenomena in the tropical atmosphere over the western Pacific. *Mon. Wea. Rev.*, **120,** 407–430.

Velasco, I., and J. M. Fritsch, 1987: Mesoscale convective complexes in the Americas. *J. Geophys. Res.*, **92,** 9591–9614.

Webster, P. J., and G. L. Stephens, 1980: Tropical upper-tropospheric extended clouds: Inferences from Winter MONEX. *J. Atmos. Sci.*, **37,** 1521–1541.

——, and R. A. Houze, Jr., 1991: The Equatorial Mesoscale Experiment (EMEX): An overview. *Bull. Amer. Meteor. Soc.*, **72,** 1481–1505.

Wielicki, B. A., and R. M. Welch, 1986: Cumulus cloud properties derived using LANDSAT satellite data. *J. Climate Appl. Meteor.*, **25,** 261–305.

Williams, M., and R. A. Houze, Jr., 1987: Satellite-observed characteristics of winter monsoon cloud clusters. *Mon. Wea. Rev.*, **115,** 505–519.